

## Towards simultaneous achievement of carrier activation and crystallinity in Ge and GeSn with heated phosphorus ion implantation: An optical study

Vijay Richard D'Costa,<sup>1,a)</sup> Lanxiang Wang,<sup>1</sup> Wei Wang,<sup>1</sup> Sin Leng Lim,<sup>2</sup> Taw Kuei Chan,<sup>2</sup> Lye Hing Chua,<sup>3</sup> Todd Henry,<sup>3</sup> Wei Zou,<sup>3</sup> Christopher Hatem,<sup>3</sup> Thomas Osipowicz,<sup>2</sup> Eng Soon Tok,<sup>2</sup> and Yee-Chia Yeo<sup>1,b)</sup>

<sup>1</sup>Department of Electrical and Computer Engineering, National University of Singapore, Singapore 117583

<sup>2</sup>Department of Physics, National University of Singapore, Singapore 117551

<sup>3</sup>Applied Materials – Varian Semiconductor Equipment, 35 Dory Road, Gloucester, Massachusetts 01930, USA

(Received 28 April 2014; accepted 12 September 2014; published online 23 September 2014)

We have investigated the optical properties of Ge and GeSn alloys implanted with phosphorus ions at 400 °C by spectroscopic ellipsometry from far-infrared to ultraviolet. The dielectric response of heated GeSn implants displays structural and transport properties similar to those of heated Ge implants. The far-infrared dielectric function of as-implanted Ge and GeSn shows the typical free carrier response which can be described by a single Drude oscillator. Bulk Ge-like critical points  $E_1$ ,  $E_1 + \Delta_1$ ,  $E_0'$ , and  $E_2$  are observed in the visible-UV dielectric function of heated Ge and GeSn indicating single crystalline quality of the as-implanted layers. Although the implantation at 400 °C recovers crystallinity in both Ge and GeSn, an annealing step is necessary to enhance the carrier activation. © 2014 AIP Publishing LLC. [<http://dx.doi.org/10.1063/1.4896507>]

Ge and GeSn are being explored as next-generation materials for both nanoelectronic and optoelectronic applications. Both materials have higher electron and hole mobilities than Si and offer the possibility of realizing high-performance metal-oxide-semiconductor field-effect-transistors compatible with Si.<sup>1,2</sup>  $\text{Ge}_{1-x}\text{Sn}_x$  with a bandgap lower than Ge extends the infrared detection capability of Ge covering all the relevant telecommunications wavelengths for  $x$  as low as 0.02.<sup>3,4</sup> Besides,  $\text{Ge}_{1-x}\text{Sn}_x$  with  $x \sim 0.10$  is a potential direct bandgap material and could be the solution to the much sought after infrared interband laser based on group-IV materials.<sup>5–7</sup>

The conventional method for dopant activation consists of room temperature (RT) implantation of dopants followed by rapid thermal annealing (RTA). Implanting a high dose at RT causes structural damage to the host crystal that leads to amorphization. High temperature annealing is needed to recover the crystallinity and to activate the carriers. This recrystallization is considered to be a major challenge in sub-20 nm Si fin field-effect-transistors (FinFETs).<sup>8</sup>

Heated implantation leaves less residual structural damage compared to RT implantation, and prevents the formation of an amorphous layer.<sup>9</sup> It was reported that the Si crystal in sub-20 nm FinFETs was completely recovered using RTA following heated implantation.<sup>10</sup> The sheet resistance of heated implant was found to be consistently lower than those of RT implants. Also, heated implantation leads to perfect crystallization in ultra-thin Si channel after annealing.<sup>11</sup>

Information on microstructure as well as active carrier concentration  $N$  of implanted layers can be obtained using spectroscopic ellipsometry. The technique has been applied to study the optical properties of Ge and GeSn alloys.<sup>6,12,13</sup>

The presence of active carriers modifies the dielectric function  $\epsilon$  of a material in the infrared region. The free carrier response can be described using a Drude oscillator from which resistivity  $\rho$  and carrier relaxation time  $\tau$  (or  $N$  and mobility  $\mu$ ) are extracted.<sup>14–16</sup> Values of  $\rho$  for *in situ* doped Ge and GeSn obtained from ellipsometry are in excellent agreement with those obtained from electrical measurements.<sup>17,18</sup> The visible-UV  $\epsilon$  of crystalline Ge and GeSn shows the critical points<sup>12</sup>  $E_1$ ,  $E_1 + \Delta_1$ ,  $E_0'$ , and  $E_2$ , which arise due to long range crystalline order. The critical points are not observed in an amorphous material.

Phosphorus ion implantation into Ge at 500 °C was reported.<sup>19</sup> Sheet resistance was found to be lower in annealed Ge implanted at 500 °C relative to RT implanted Ge. Heated implantation of phosphorus into GeSn has not been reported yet. Also, an optical study of phosphorus ion implantation into heated Ge is not available. In this letter, we report the optical properties of Ge and GeSn implanted with phosphorus at 400 °C. Activation of implanted phosphorus and the preservation of crystalline structure have been confirmed by combining infrared ellipsometry with visible-UV spectroscopic ellipsometry.

Pseudomorphic  $\text{Ge}_{1-x}\text{Sn}_x$  alloys with  $x = 0.02$  and 0.06 and thicknesses between 160 and 200 nm were grown directly on Ge (100) substrates using molecular beam epitaxy.<sup>13</sup> Phosphorus was implanted into Ge substrate and GeSn alloys at 400 °C. RT implantation of phosphorus into Ge and GeSn was also done for comparison. Implant energy was 10 keV or 20 keV at a constant dose of  $2 \times 10^{15} \text{ cm}^{-2}$ . Few samples implanted at 20 keV were annealed to enhance carrier activation. Fig. 1(a) shows phosphorus profiles obtained by secondary-ion-mass-spectroscopy (SIMS) for 10 keV as-implanted Ge and GeSn. Phosphorus profiles are very similar in both Ge and GeSn at either implantation temperature. We verified that the phosphorus profile in Ge simulated using the SRIM software package<sup>20</sup> is in

<sup>a)</sup>Electronic mail: elevrd@nus.edu.sg

<sup>b)</sup>Electronic mail: eleyeoyc@nus.edu.sg

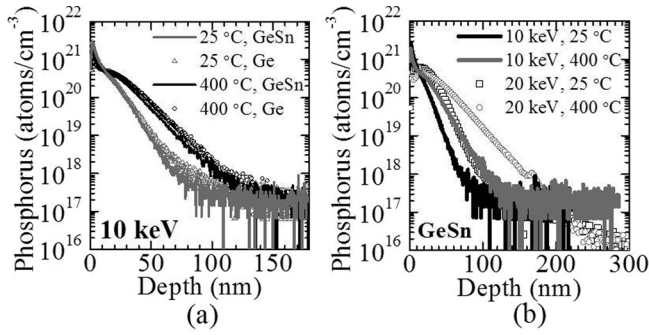


FIG. 1. (a) SIMS profiles of phosphorus implanted into Ge and  $\text{Ge}_{0.98}\text{Sn}_{0.02}$  at RT (25°C) and 400°C and at an energy of 10 keV. (b) SIMS profiles of phosphorus implanted at 10 keV and 20 keV into  $\text{Ge}_{0.98}\text{Sn}_{0.02}$  at 25°C and 400°C. As-implanted profiles were obtained.

agreement with experimental profiles, with a peak that is  $\sim 11$  nm below the surface for 10 keV implanted Ge. Heated implantation causes broadening of the phosphorus profiles relative to RT implantation. 10 keV implanted samples have shallower profiles compared to 20 keV implanted samples [Fig. 1(b)].

Spectroscopic ellipsometry measurements were carried out using J. A. Woollam's infrared variable angle spectroscopic ellipsometer (IR-VASE) and a variable angle spectroscopic ellipsometer (VASE). The ellipsometric angles  $\Psi$  and  $\Delta$  were acquired at an angle of incidence of  $65^\circ$  from 0.05 to 0.65 eV and 1.3 to 4.7 eV on IR-VASE and VASE, respectively. The imaginary part of pseudo-dielectric function  $\langle \epsilon_2 \rangle$  for Ge and GeSn is shown in Fig. 2.  $\langle \epsilon_2 \rangle$  shows enhanced absorption in the far-infrared for heated Ge and GeSn implants compared to RT implants. The principal distinguishing characteristic of heated implants with respect to RT implants in the visible-UV response is the observation of  $E_1$ ,

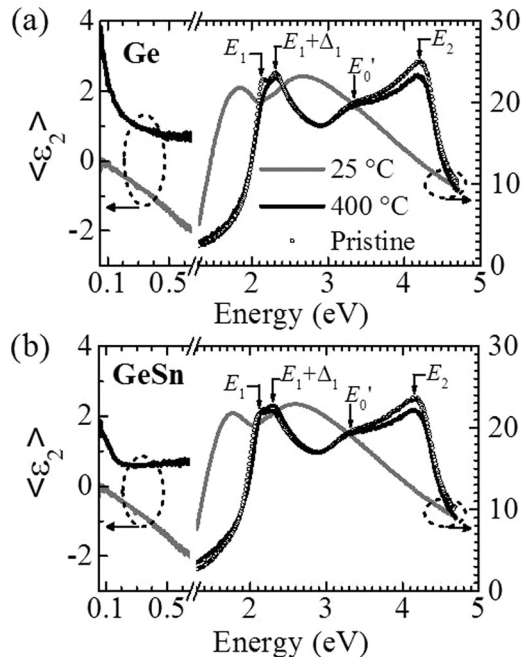


FIG. 2.  $\langle \epsilon_2 \rangle$  for 10 keV implanted (a) Ge and (b)  $\text{Ge}_{0.98}\text{Sn}_{0.02}$  at 25°C and 400°C. Visible-UV dielectric response of pristine Ge and  $\text{Ge}_{0.98}\text{Sn}_{0.02}$  is also shown for comparison with heated implants. The legend applies to both plots.

$E_1 + \Delta_1$ ,  $E_0'$ , and  $E_2$  indicating crystalline single-phase quality of the implanted layers. The preservation of crystalline structure leads to more channeling in heated implants, accounting for the broadening of phosphorus profiles observed in Fig. 1. Visible-UV  $\langle \epsilon_2 \rangle$  for RT implanted samples shows the typical broad peak  $\sim 3$  eV and an additional peak below 2 eV. The peak at lower energy is related to the thickness of the amorphous layer.

To investigate in detail, the optical response of heated implants, we modeled GeSn samples with a four-layer system consisting of Ge substrate, pristine GeSn film,  $n$ -GeSn film, and a surface layer.<sup>13</sup> A three-layer system consisting of Ge substrate,  $n$ -Ge, and surface layer was used for Ge samples. The surface layer was modeled as a  $\text{GeO}_2$  layer in the visible-UV range.<sup>21</sup> A rough layer was used in the infrared range where the oxide optical constants are not known.<sup>18</sup> The pre-implanted Ge substrate and GeSn films were characterized separately, and the dielectric function obtained was used in tabulated form in the model. The infrared dielectric function of heated Ge and GeSn was described using<sup>18</sup>

$$\epsilon(E) = C + \frac{-\hbar^2}{\epsilon_0 \rho (\tau E^2 + i\hbar E)} + \frac{A_{\text{pole}}}{(E_{\text{pole}}^2 - E^2)}, \quad (1)$$

where the parameters  $C$ ,  $A_{\text{pole}}$ , and  $E_{\text{pole}}$  are defined in Ref. 18. The second term in Eq. (1) is the Drude oscillator. The third term accounts for the dispersion caused by absorption outside the measured spectral range. Since the carrier distribution in the implanted layers could be non-homogeneous,<sup>22–26</sup> it is convenient to express Eq. (1) in terms of  $N$  and  $\mu$  to investigate the carrier profiles. We used  $\rho = \frac{1}{e\mu N}$  and  $\tau = \frac{m^* \mu}{e}$  in Eq. (1).  $m^*$  is  $0.14 m_e$  and  $0.12 m_e$  for Ge and GeSn, respectively.<sup>17</sup> The data were first analyzed using the procedure described in Ref. 18 assuming uniform  $N$ . This allows us to estimate average  $\rho$  and  $N$  (or active dose) for quick evaluation of the implanted layers. The infrared response of RT implanted Ge and GeSn did not require the presence of Drude oscillator in Eq. (1). This confirms that the enhanced infrared absorption observed in Ge and GeSn heated implants is caused by the presence of free charge carriers. We found that either complementary error profile,<sup>22</sup>

$N_{CE}(d) = N_{\text{max}} \text{erfc}\left(\frac{1}{2\sqrt{Dt}}d\right)$  or Gaussian profile,<sup>16</sup>  $N_G(d) = N_{\text{max}} \exp\left(-\left(\frac{d-R_p}{\sqrt{2}\Delta R_p}\right)^2\right)$  provided equally good fit to infrared

$\langle \epsilon \rangle$  of as-implanted samples.  $N_{\text{max}}$  is the maximum carrier concentration for both profiles and  $Dt$  is the diffusivity-time product.  $R_p$  and  $\Delta R_p$  are range and standard deviation of the Gaussian profile, respectively. The mobility was described

by  $\mu(d) = \mu_{\text{max}} / \left(1 + \sqrt{\frac{N(d)}{10^{17}}}\right)$ .<sup>27</sup> The fit to  $\langle \epsilon \rangle$  of heated Ge

with various carrier profiles is shown in Fig. 3(a). The inset in Fig. 3(a) indicates improvement achieved for the model with a non-uniform profile.  $N_{CE}(d)$  appears to be the best solution based on mean square error (MSE) although it is hard to distinguish between the two model fits with non-uniform profile. Fig. 3(b) shows the extracted carrier profiles.  $N_G(d) \sim N_{CE}(d)$  as may be expected from the equivalence of their line-shapes.<sup>22</sup> The results for 10 keV heated Ge and

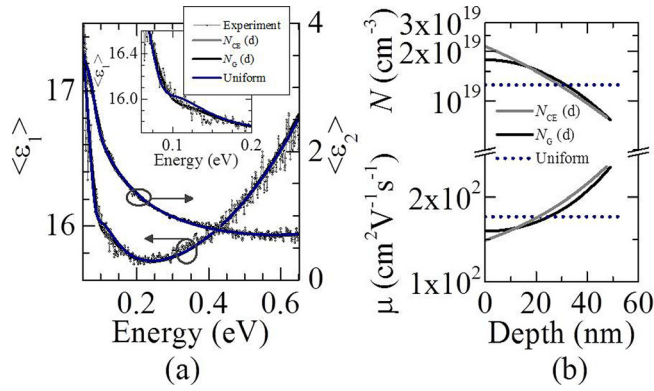


FIG. 3. Infrared real and imaginary parts of (a) experimental and modeled pseudo-dielectric function for 10 keV implanted Ge at 400 °C and (b) Carrier concentration and mobility profiles for 10 keV as-implanted Ge at 400 °C.

GeSn are summarized in Table I. We are not able to obtain unique set of model parameters for as-implanted GeSn, which has thickness of underlying pristine GeSn layer as an additional fit parameter. However, unique carrier profiles can be extracted for annealed GeSn, where the experimental data are sensitive to all the parameters. Our systematic study of as-implanted, annealed, and *in situ* doped Ge samples indicates that active dose is the most robust parameter irrespective of the carrier profile used to describe the infrared response. We will use average  $N$  and  $\mu$  (or  $\rho$  and  $\tau$ ) for a comparative study between Ge and GeSn. We obtained  $\rho = 3.6 \pm 0.7$  m $\Omega$ -cm and  $\tau = 11 \pm 3$  fs for 10 keV and 20 keV as-implanted Ge ( $N = 1.4 \times 10^{19}$  cm<sup>-3</sup>,  $\mu = 141$  cm<sup>2</sup>V<sup>-1</sup>s<sup>-1</sup>).  $\rho$  is  $\sim 50\%$  higher compared to bulk Ge resistivity<sup>25</sup> for  $1.4 \times 10^{19}$  cm<sup>-3</sup> which could be attributed to the incomplete recovery of the Ge crystal. The thinner implanted layer may also contribute to higher  $\rho$  and lower  $\tau$  or lower  $\mu$ .<sup>28</sup> As-implanted GeSn gave higher  $\rho = 11 \pm 1$  m $\Omega$ -cm and lower  $\tau = 8 \pm 2$  fs ( $N \sim 5 \times 10^{18}$  cm<sup>-3</sup> and  $\mu \sim 117$  cm<sup>2</sup>V<sup>-1</sup>s<sup>-1</sup>) compared to Ge. It should be pointed out that  $\rho$  and  $\tau$  for GeSn heated implants match with those for the as-grown *in situ* doped *n*-type GeSn.<sup>17</sup>  $\rho$  and  $\tau$  of *in situ* doped GeSn films was improved further by annealing indicating that a further annealing step is necessary in our heated implants including Ge.

TABLE I. Carrier profile parameters for 10 keV as-implanted Ge and GeSn at 400 °C.  $t_i$  is the thickness of the implanted layer.

Parameters	Ge			GeSn
	$N_{CE}$ (d)	$N_G$ (d)	Uniform	Uniform
MSE	0.451	0.453	0.459	0.462
$t_i$ (nm)	$48 \pm 1$	$49 \pm 1$	$55 \pm 1$	$81 \pm 6$
$N_{max}$ ( $10^{19}$ cm <sup>-3</sup> )	$2.1 \pm 0.2$	$1.7 \pm 0.1$	...	...
$Dt$ (nm <sup>2</sup> )	$1386 \pm 243$	...	...	...
$R_p$ (nm)	...	0	...	...
$\Delta R_p$ (nm)	...	$38 \pm 3$	...	...
$\mu_{max}$ (cm <sup>2</sup> V <sup>-1</sup> s <sup>-1</sup> )	$2333 \pm 40$	$2277 \pm 36$	...	...
$N$ ( $10^{19}$ cm <sup>-3</sup> )	1.4	1.4	$1.3 \pm 0.1$	$0.37 \pm 0.02$
$\mu$ (cm <sup>2</sup> V <sup>-1</sup> s <sup>-1</sup> )	185	182	$177 \pm 2$	$141 \pm 2$
Active dose ( $10^{15}$ cm <sup>-2</sup> )	0.0675	0.0676	0.0683	0.0297
Efficiency (%)	$\sim 3.4$	$\sim 3.4$	$\sim 3.4$	$\sim 1.5$

The UV-visible  $\epsilon$  of heated Ge and GeSn implants was analyzed using the procedure described in Ref. 13 with the starting thickness values in the fitting taken from infrared ellipsometry measurements. As suggested by  $\langle \epsilon_2 \rangle$  in Fig. 2, the extracted UV-visible  $\epsilon$  of heated Ge and GeSn implants is very similar to  $\epsilon$  of bulk Ge and intrinsic GeSn alloys. We carried out a critical point analysis to investigate the effect of implantation temperature and doping on  $E_1$ ,  $E_1 + \Delta_1$ ,  $E'_0$ , and  $E_2$ . The derivatives of the experimental dielectric function were fitted using  $\frac{d^2\epsilon}{dE^2} = \sum_j \frac{A_j e^{i\Phi_j}}{[E - E_j + i\Gamma_j]^2}$  where  $A_j$ ,  $\Phi_j$ ,  $E_j$ , and  $\Gamma_j$  are the amplitude, phase angle, transition energy, and broadening parameter, respectively.<sup>6</sup> The summation covers  $E_1$ ,  $E_1 + \Delta_1$ ,  $E'_0$ , and  $E_2$ . We followed the procedure in Ref. 6 for fitting the derivatives. Fig. 4 shows the derivative features corresponding to  $E_1$ ,  $E_1 + \Delta_1$ , and  $E_2$  in pristine and 400 °C implanted Ge and GeSn.  $E_1$  and  $E_1 + \Delta_1$  in implanted GeSn appear to match pristine GeSn better than Ge indicating that 400 °C might be closer to the optimal temperature for heated implantation in GeSn. Our results also suggest that implanted GeSn layer is of good crystalline quality.

Fig. 5(a) shows 2 MeV He<sup>+</sup> Rutherford backscattering (RBS) random and aligned spectra for both 400 °C implanted and pristine GeSn alloy. Implanted GeSn shows high degree of channeling comparable to the pristine sample indicating that the implanted layer is indeed monocrystalline. The crystal damage resulting from phosphorus implantation at 400 °C appears to be annealed out. In addition, Fig. 5(a) indicates that the Sn profile in implanted sample is identical to the pristine GeSn alloy. The difference in broadening parameter,  $\Delta\Gamma$  of heated implants for  $E_2$  is 20 meV for Ge and 16 meV for GeSn with respect to the values in their pristine state.  $\Delta\Gamma$  for the average of  $E_1$  and  $E_1 + \Delta_1$  relative to their pristine counterparts is 29 meV and 3 meV for Ge and GeSn, respectively.  $\Delta\Gamma$  is smaller for the 400 °C implanted GeSn compared to Ge, which is also consistent with the closeness of  $E_1$  and  $E_1 + \Delta_1$  derivatives in implanted and pristine GeSn compared to Ge. Besides doping, the incomplete recovery of the

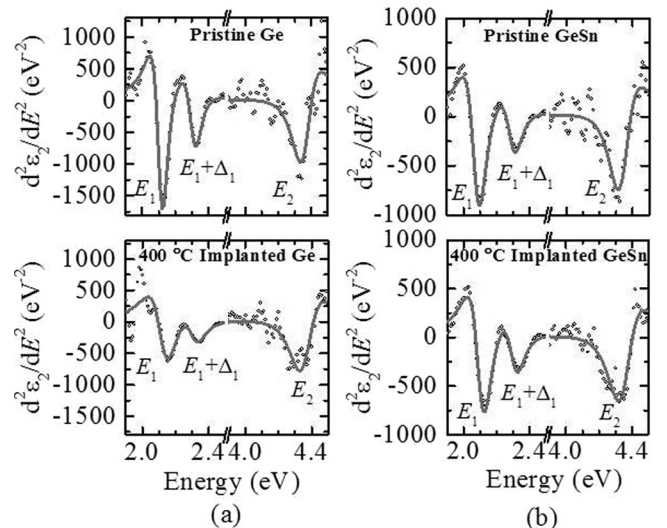


FIG. 4. Numerical second derivatives of visible-UV  $\epsilon_2$  for pristine and implanted (a) Ge and (b) Ge<sub>0.98</sub>Sn<sub>0.02</sub> at 10 keV and 400 °C. Experimental data are plotted in circles, and the model is plotted using solid lines.

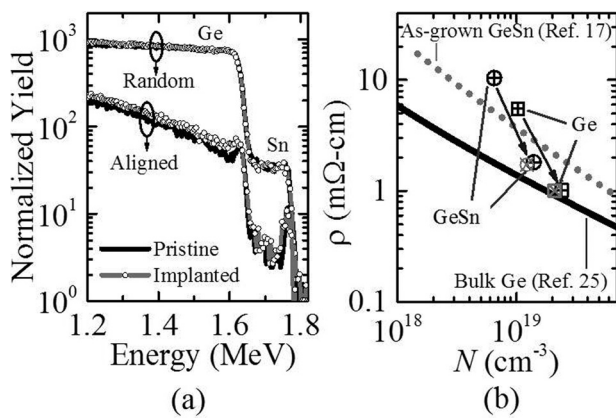


FIG. 5. (a) 2 MeV  $\text{He}^+$  RBS random and aligned spectra for pristine and 10 keV implanted  $\text{Ge}_{0.98}\text{Sn}_{0.02}$  at 400 °C. RBS aligned spectra were acquired at normal incidence [100]. (b)  $\rho$  plotted as a function of  $N$  for 20 keV implanted Ge and GeSn. The gray circles and squares correspond to annealed RT implanted Ge and GeSn. The black circles and squares correspond to 400 °C implanted Ge and GeSn. The arrows indicate the lowering of  $\rho$  and enhancement in  $N$  post-annealing of 400 °C implanted Ge and GeSn.

crystal could also contribute to the broadening parameter in implanted layers. In heavily doped bulk Ge,<sup>29</sup>  $N$  of  $5 \times 10^{18} \text{ cm}^{-3}$  and  $1.4 \times 10^{19} \text{ cm}^{-3}$  enlarges the broadening parameter by  $\sim 5 \text{ meV}$  and  $\sim 10 \text{ meV}$ , respectively, relative to pure Ge. Doping in implanted Ge could account for half of the observed broadening shift for the average of  $E_1$  and  $E_1 + \Delta_1$  whereas the rest may be attributed to incomplete recovery of Ge to its pristine state. Heated implantation at 400 °C in GeSn appears to recover crystallinity more effectively compared to Ge for the implantation dose used in our experiments. This is analogous to heated implantation at higher temperature that is needed in Si to maintain crystallinity compared to Ge.<sup>9</sup> The 20 keV as-implanted Ge and GeSn show a red-shift in  $E_1$ ,  $E_1 + \Delta_1$ , and  $E_2$  energies as observed in heavily doped bulk Ge<sup>29</sup> with respect to pure Ge. However, a small blue-shift in  $E_1$ ,  $E_1 + \Delta_1$ , and  $E_2$  is observed in both 10 keV implanted Ge and GeSn. These results for 10 keV implanted samples appear to follow the trend found in heavily doped and strongly compensated Ge films.<sup>30</sup> A blue-shift was reported for  $E_0$  and  $E_1$  with respect to intrinsic Ge. A detailed investigation may be needed to understand the trends in the energy shifts found in our implanted samples.

Fig. 5(b) shows  $\rho$  as a function of  $N$  for 20 keV implanted Ge and GeSn.  $\rho$  for both as-implanted Ge and GeSn at 400 °C is closer to *in situ* doped as-grown GeSn than bulk Ge. The implanted layers were annealed at 450 °C for duration of 180 s. Lower  $\rho$  and higher  $N$  relative to heated implants was achieved by RTA of implanted layers formed by RT implantation. Further, optimization is needed to achieve high carrier activation in heated implantation. Upon annealing, heated Ge and GeSn implants give bulk Ge-like  $\rho$  and  $N$  which are very close to the annealed RT implants. This is despite the fact that heated implants have active carriers prior to annealing compared to RT implants. However, heated implantation does preserve crystallinity in the implanted layer which is found to be critical in ultra-thin Si channel and sub-20 nm FinFETs where the lack of sufficient crystalline seed leads to incomplete recovery of crystal damage.

In conclusion, we studied the optical response of phosphorus implanted Ge and GeSn alloys using spectroscopic ellipsometry. The dielectric function of implanted GeSn obtained from far-infrared to ultraviolet displays characteristics similar to implanted Ge. Heated implantation leads to a crystalline film and also results in activation of carriers. However, an annealing step is needed to improve  $\rho$  and  $N$ . The results and analysis suggest that the optimum implantation temperature for GeSn may be close to 400 °C but further optimization may be needed to maximize carrier activation in GeSn.

This work was supported by the National Research Foundation under the Competitive Research Programme (Grant No. NRF-CRP6-2010-4).

- <sup>1</sup>X. Gong, G. Han, F. Bai, S. Su, P. Guo, Y. Yang, R. Cheng, D. Zhang, G. Zhang, C. Xue, B. Cheng, J. Pan, Z. Zhang, E. S. Tok, D. Antoniadis, and Y.-C. Yeo, *IEEE Electron Device Lett.* **34**(3), 339 (2013).
- <sup>2</sup>S. Gupta, R. Chen, J. S. Harris, and K. C. Saraswat, *Appl. Phys. Lett.* **103**(24), 241601 (2013).
- <sup>3</sup>V. R. D'Costa, Y. Fang, J. Mathews, R. Roucka, J. Tolle, J. Menéndez, and J. Kouvetakis, *Semicond. Sci. Technol.* **24**(11), 115006 (2009).
- <sup>4</sup>J. Mathews, R. Roucka, J. Xie, S. Q. Yu, J. Menéndez, and J. Kouvetakis, *Appl. Phys. Lett.* **95**(13), 133506 (2009).
- <sup>5</sup>R. Chen, H. Lin, Y. Huo, C. Hitzman, T. I. Kamins, and J. S. Harris, *Appl. Phys. Lett.* **99**(18), 181125 (2011).
- <sup>6</sup>V. R. D'Costa, C. S. Cook, A. G. Birdwell, C. L. Littler, M. Canonico, S. Zollner, J. Kouvetakis, and J. Menendez, *Phys. Rev. B* **73**(12), 125207 (2006).
- <sup>7</sup>J. P. Gupta, N. Bhargava, S. Kim, T. Adam, and J. Kolodzey, *Appl. Phys. Lett.* **102**(25), 251117 (2013).
- <sup>8</sup>R. Duffy, M. J. H. Van Dal, B. J. Pawlak, M. Kaiser, R. G. R. Weemaes, B. Degroote, E. Kunnen, and E. Altamirano, *Appl. Phys. Lett.* **90**(24), 241912 (2007).
- <sup>9</sup>J. W. Mayer, L. Eriksson, and J. A. Davies, *Ion Implantation in Semiconductors: Silicon and Germanium* (Academic Press, New York, 1970).
- <sup>10</sup>M. Togo, Y. Sasaki, G. Zschatzsch, G. Boccardi, R. Ritzenthaler, J. W. Lee, F. Khaja, B. Colombeau, L. Godet, P. Martin, S. Brus, S. E. Altamirano, G. Mannaert, H. Dekkers, G. Hellings, N. Horiguchi, W. Vandervorst, and A. Thean, *IEEE Symp. VLSI Technol.* **2013**, T196.
- <sup>11</sup>W. Mizubayashi, H. Onoda, Y. Nakashima, Y. Ishikawa, T. Matsukawa, K. Endo, Y. X. Liu, S. O'uchi, J. Tsukada, H. Yamauchi, S. Migita, Y. Morita, H. Ota, and M. Masahara, *IEEE Int. Electron Devices Meet.* **2013**, 538.
- <sup>12</sup>L. Viña, S. Logothetidis, and M. Cardona, *Phys. Rev. B* **30**(4), 1979 (1984).
- <sup>13</sup>V. R. D'Costa, W. Wang, Q. Zhou, E. S. Tok, and Y.-C. Yeo, *Appl. Phys. Lett.* **104**(2), 022111 (2014).
- <sup>14</sup>M. Schubert, *Infrared Ellipsometry on Semiconductor Layer Structures: Phonons, Plasmons, and Polaritons* (Springer, 2004).
- <sup>15</sup>T. Hofmann, C. M. Herzinger, T. E. Tiwald, J. A. Woollam, and M. Schubert, *Appl. Phys. Lett.* **95**(3), 032102 (2009).
- <sup>16</sup>T. E. Tiwald, D. W. Thompson, J. A. Woollam, W. Paulson, and R. Hance, *Thin Solid Films* **313-314**, 661 (1998).
- <sup>17</sup>V. R. D'Costa, J. Tolle, J. Xie, J. Menéndez, and J. Kouvetakis, in *American Institute of Physics Conference Series* (2010), Vol. 1199, pp. 57.
- <sup>18</sup>V. R. D'Costa, J. Tolle, J. Xie, J. Kouvetakis, and J. Menéndez, *Phys. Rev. B* **80**(12), 125209 (2009).
- <sup>19</sup>M. A. Razali, A. J. Smith, C. Jeynes, and R. M. Gwilliam, *AIP Conf. Proc.* **1496**, 193 (2012).
- <sup>20</sup>J. F. Ziegler, J. P. Biersack, and M. D. Ziegler, *SRIM, the Stopping and Range of Ions in Matter* (Lulu Press, 2008).
- <sup>21</sup>Y. Z. Hu, J. T. Zettler, S. Chongsawangvirod, Y. Q. Wang, and E. A. Irene, *Appl. Phys. Lett.* **61**(9), 1098 (1992).
- <sup>22</sup>J. C. Irvin, *Bell Syst. Tech. J.* **41**(2), 387 (1962).
- <sup>23</sup>H. H. Wagner and R. R. Schaefer, *J. Appl. Phys.* **50**(4), 2697 (1979).
- <sup>24</sup>E. Tannenbaum, *Solid-State Electron.* **2**(2), 123 (1961).
- <sup>25</sup>D. B. Cuttriss, *Bell Syst. Tech. J.* **40**, 509 (1961).

<sup>26</sup>T. Abe and T. Kato, *Jpn. J. Appl. Phys., Part 1* **4**(10), 742 (1965).

<sup>27</sup>C. Hilsum, *Electron. Lett.* **10**(13), 259 (1974).

<sup>28</sup>V. R. D'Costa, S. Subramanian, D. Li, S. Wicaksono, S. F. Yoon, E. S. Tok, and Y.-C. Yeo, *Appl. Phys. Lett.* **104**(23), 232102 (2014).

<sup>29</sup>L. Viña and M. Cardona, *Phys. Rev. B* **34**(4), 2586 (1986).

<sup>30</sup>N. P. Garbar, L. A. Matveeva, V. F. Mitin, Y. A. Tkhonik, R. Harman, Y. M. Shvarts, and Z. Stroubek, *Sov. Phys. Semicond.* **21**(3), 245 (1987).